A MOEMS ACCELEROMETER BASED ON DIFFRACTION GRATING WITH IMPROVED MECHANICAL STRUCTURE

*Qianbo Lu, Wenxiu Lian ,Shuqi Lou, Chen Wang, Jian Bai*and Guoguang Yang*
State Key Laboratory of Modern Optical Instrumentation, Zhejiang University, Hangzhou 310027, China
** Corresponding author: bai@zju.edu.cn*

Abstract: (250 Words)
In this paper, an improved MOEMS accelerometer is described, which is based on integrated grating with phase modulation. This device is composed of a laser diode, an optoelectronic processing circuit and a sensing chip consisted of a piezoelectric translator, an integrated grating as a reflective mirror on a transparent substrate and a mechanical part of a bulk silicon proof mass suspended by four cantilevers whose upper surface acted as another mirror. This device generates a series of interference fringes by two diffracted beams when illuminated with coherent light, whose intensities are modulated by the relative distance between the grating and the proof mass. The intensities of the interference fringes varied with the distance alteration caused by external accelerations, which is proportional to the acceleration. It is realizable to get the magnitude of acceleration by using a differential circuit to detect the distance. A modified structure is introduced in this paper to obtain high sensitivity and reduce cross-sensitivity between different sensitive axes. Compared to experimental results before the simulation and theory analysis demonstrate that this modified MOEMS accelerometer has a good performance with higher static acceleration sensitivity of 3×10^3V/g and very low crosstalk.

Keywords: MOEMS, optical interferometry, diffraction grating, mechanism improvement

1. INTRODUCTION

Accelerometers exploit their wide applications in various fields like vibration measurement of vehicles, seismic monitoring, inertial navigation, and attitude controlling [1-4]. They have been successfully applied in our daily lives as well, such as portable devices, game controllers, and automobiles. In recent years, MEMS (Micro-Electronic Mechanical System) accelerometers have received considerable interest due to their small size and low cost. However, the working principles of the commercial MEMS accelerometers are mainly piezoresistive and capacitive as well as the traditional ones and they suffer from inherent drawbacks such as temperature dependence, low sensitivity and high cross-sensitivity to electromagnetic interference and so on. MOEMS (Micro-Optical Electronic Mechanical System) accelerometers, are especially attractive devices compared to conventional piezoresistive or capacitive accelerometers, because they have advantages of immunity to electromagnetic interference, high sensitivity and remote sensing etc. There have been some typical demonstrations of MOEMS accelerometers [5-7] with the method such as Fabry-Pérot cavity and Michelson Optical interferometry combining with electrical and mechanical design is an ideal way to achieve a high sensitivity of displacement and acceleration. In addition, optical accelerometers offer the possibility of force-feedback for larger dynamic range and bandwidth. Optical accelerometers that use Fabry-Pérot cavity technology can provide navigation-grade accuracy at low cost [8-10]. Those MOEMS accelerometers using diffraction grating can even achieve tens of ng/$\sqrt{Hz}$ [11-12]. Interdigital phase-sensitive diffraction gratings enable implementation of interferometric detection in sensitive micromachined accelerometers [13-15].

In this paper, a modified MOEMS accelerometer based on diffraction grating with phase modulation technique is proposed. The principle of detection and the modified mechanical design is introduced.

2. PRINCIPLE OF DETECTION

In this paper, a scheme of the acceleration measuring principle based on grating interferometer and phase modulation technique is proposed. In general, the basic sensing principle of conventional accelerometer is to measure the displacement of cantilevers mounted to a proof mass bought by acceleration with electric or optical methods. The proposed accelerometer also uses this basic sensing principle, which can be expressed by formula: $F=ma$. In this section, I first explain the interferometer based on grating and then introduce the phase modulation which can greatly increase the resolution of acceleration detection.

2.1 The interferometer based on grating

As is shown in figure 1, the grating interferometer is achieved by a diffraction grating and a reflecting mirror. In this schematic, the grating also acts as a beam splitter and d is the distance between the grating and reflecting mirror.

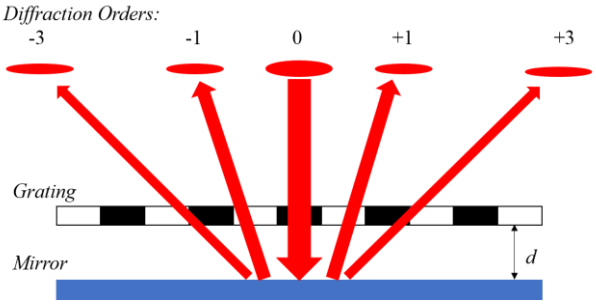

Fig. 1: Schematic diagram of the interferometer based on grating

When a coherent laser beam illuminates the grating normally, a portion of the incident light is reflected and diffracted directly from the grating while the other portion travels through the grating and reflects from the mirror. These two reflected beams with diffraction due to the grating interfere coherently, creating a diffracted field consisting of zero and high orders whose angles remain fixed but intensities modulated by the displacement between the

grating and mirror. The top surface of the proof mass, coated with aluminum, serves as a reflecting mirror.

A simple analysis of the relationship between the intensities of diffraction orders and the distance between the grating and proof mass can be deduced.

The plural amplitude can be expressed by Franuhofer diffraction theory as this case meets its scope of application [18].

$$E(p) = C \int_{grating} F' e^{-jkpx} dx \tag{1}$$

Where $E(p)$ is the plural amplitude of diffraction, and $k = 2\pi/\lambda$ is the wave vector, C is normalization constant, F' is the transfer function of the grating, $p = \sin\theta_i - \sin\theta_o$, while θ_i and θ_o is the angle of incidence and diffraction respectively. Because of the periodicity of the grating, equation (1) can be rewritten as:

$$\begin{aligned} E(p) &= \sum_{n=0}^{N-1} e^{-jkpx_n} C \int_{period} F e^{-jkpx} dx \\ &= \frac{1-e^{-jNkp\Lambda}}{1-e^{-jkp\Lambda}} C \int_{period} F e^{-jkpx} dx \end{aligned} \tag{2}$$

Where N is the number of period of the grating, and F is the transfer function in one period, it can be expressed as:

$$F = \begin{cases} e^{-j\frac{\theta}{2}}, \frac{\Lambda}{4} < |x| < \frac{3\Lambda}{4} \\ e^{j\frac{\theta}{2}}, -\frac{\Lambda}{4} < x < \frac{\Lambda}{4} \end{cases} \tag{3}$$

Where θ is given by following analysis formula:

$$\theta = \frac{2\pi}{\lambda} d\left(\frac{1}{\cos\theta_0} + \frac{1}{\cos\theta_i}\right) \tag{4}$$

As this accelerometer is approximately under the normal incidence condition, the $\theta_o = 0$ and $\cos\theta_i \approx 1$. Equation (4) has the following estimation:

$$\theta = \frac{4\pi}{\lambda} d \tag{5}$$

The plural amplitude of diffraction in one period then becomes:

$$\begin{aligned} E_d(p) &= C\int_{\Lambda} F e^{-jkpx} dx \\ &= \frac{E_0}{N}\left(\cos\frac{\theta}{2}\frac{\sin kp\frac{\Lambda}{2}}{kp\frac{\Lambda}{2}} - j\sin\frac{\theta}{2}\left(\frac{\sin kp\frac{\Lambda}{2}}{kp\frac{\Lambda}{2}} - \frac{\sin kp\frac{\Lambda}{4}}{kp\frac{\Lambda}{4}}\right)\right) \end{aligned} \tag{6}$$

Where $E_0 = CN\Lambda$, is the incident plural amplitude of diffraction. Therefore, we can express the intensity of interference orders as:

$$\begin{aligned} I(p) &= E(p)E(p)^* \\ &= \left(\frac{\sin N\frac{kp\Lambda}{2}}{\sin\frac{kp\Lambda}{2}}\right)^2 |E_d(p)|^2 \end{aligned} \tag{7}$$

Combining equation (6) and equation (7) yields the intensity:

$$I(p) = \frac{I_{in}}{N^2}\frac{\sin^2 N\frac{kp\Lambda}{2}}{\sin^2\frac{kp\Lambda}{2}}\left(\begin{aligned} &\cos^2\frac{\theta}{2}\sin c^2\frac{kp\Lambda}{2} + \\ &\sin^2\frac{\theta}{2}\left(\sin c\frac{kp\Lambda}{2} - \sin c\frac{kp\Lambda}{4}\right)^2 \end{aligned}\right) \tag{8}$$

Where I_{in} is the intensity of incident light. When $kp = 0$, the zero order interferential diffraction intensity can be described:

$$I_0(kp=0) = I_{in}\cos^2\frac{\theta}{2} = \frac{I_{in}}{2}(1+\cos\theta) \tag{9}$$

The *n*th order interferential diffraction intensity is given as:

$$I_n(kp\Lambda = 2n\pi) = \frac{I_{in}}{2}(1-\cos\theta)\sin c^2\frac{n\pi}{2} \tag{10}$$

Thus, a simple analysis of the reflected field shows that the diffraction order intensities I_0, $I_{\pm1}$ and $I_{\pm3}$ can be expressed as a function of the displacement between the grating and proof mass, d.

$$\begin{aligned} I_0 &= \frac{I_{in}}{2}\left(1+\cos\frac{4\pi d}{\lambda}\right) = I_{in}\cos^2\left(\frac{2\pi}{\lambda}d\right) \\ I_{\pm1} &= \frac{2I_{in}}{\pi^2}\left(1-\cos\frac{4\pi d}{\lambda}\right) = \frac{4I_{in}}{\pi^2}\sin^2\left(\frac{2\pi}{\lambda}d\right) \\ I_{\pm3} &= \frac{2I_{in}}{9\pi^2}\left(1-\cos\frac{4\pi d}{\lambda}\right) = \frac{4I_{in}}{9\pi^2}\sin^2\left(\frac{2\pi}{\lambda}d\right) \end{aligned} \tag{11}$$

Equation (11) shows that the intensity of each diffraction order is a periodic function of the displacement. We can use any of these diffraction orders to measure the displacement, and then get the acceleration variety.

2.2 The Phase modulation

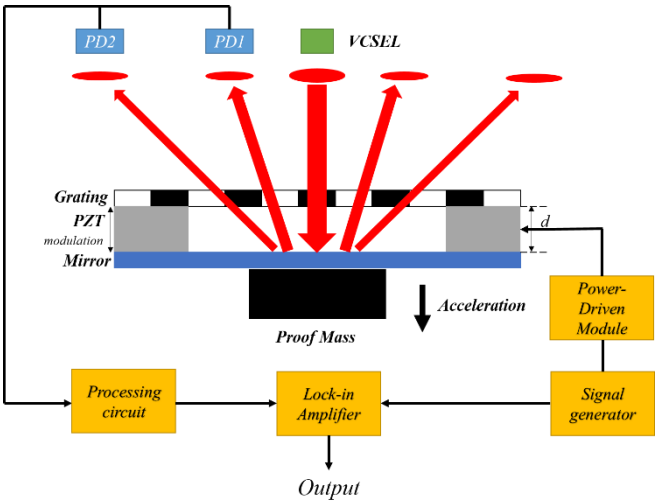

Fig. 2: Schematic of the proposed accelerometer

The realization of the phase modulation requires a piezoelectric translator, a signal generator, a power-driven module, a processing circuit and a lock-in amplifier, as shown in figure 2. The grating is fixed on the PZT, which is driven by the signal generator and power-driven module. The displacement between the grating and mirror can be modulated by applying a signal voltage to the PZT.

Two identical signals from the signal generator are sent to the power-driven module and the lock-in amplifier. The one is to drive the PZT while the other is as the reference signal. The imported phase by the PZT can be expressed as:

$$\varphi' = M\sin\omega' t \tag{12}$$

Where M is the modulation depth and ω' is the modulation frequency. The intensity of the ±1 orders can be written as:

$$\begin{aligned} I_{\pm1}(d) &= \frac{2I_{in}}{\pi^2}\left[1-\cos\left(\frac{4\pi d}{\lambda}+\varphi'\right)\right] \\ &= \frac{2I_{in}}{\pi^2}\left[1-\cos\left(\frac{4\pi d}{\lambda}+M\sin\omega' t\right)\right] \end{aligned} \tag{13}$$

Using Bessel function and transformation of triangle function equation (13) can be rewritten as:

$$I_{\pm 1}(d)=\frac{2I_{in}}{\pi^2}\left[\begin{array}{l}1-\cos(\frac{4\pi d}{\lambda})(J_0(M)+2J_2(M)\cos 2\omega' t+\cdots)\\+\sin(\frac{4\pi d}{\lambda})(2J_1(M)\sin\omega' t+2J_3(M)\sin 3\omega' t+\cdots)\end{array}\right] \quad (14)$$

After detection by the PD and amplified by the conditioning circuit, the intensity converts to the voltage $V_{sig} = \Omega \times S \times I_{\pm 1}$, where S is the responsivity of PD and Ω is the gain of signal conditioning circuit. The reference voltage from the signal generator is $V_{ref} = R\sin\omega' t$, where R is the reference amplitude. Through the lock-in amplifier, the output voltage is a DC signal in a certain acceleration:

$$\begin{aligned}V_{out}&=\frac{4\Omega SRI_{in}}{\pi^2}J_1(M)\sin\frac{4\pi d}{\lambda} \quad (15)\\&=\frac{4\Omega SRI_{in}}{\pi^2}J_1(M)\sin\frac{4\pi}{\lambda}(d_0+\Gamma\bullet a)\end{aligned}$$

Equation (15) indicates the relationship between the output and acceleration a. Employing phase modulation technique can effectively suppress the noise and derive the faint signal, finally improve SNR of the accelerometer.

3. MODIFIED MECHANICAL DESIGN

Traditional accelerometer besides this MOMES accelerometer can be considered as a second-order harmonic oscillator system:

$$m\frac{d^2x}{dt^2}+c\frac{dx}{dt}+kx=ma \quad (16)$$

Where m is the proof mass, a is acceleration, c is the damping coefficient, k is the elastic coefficient of this structure, and x is the displacement of the proof mass. Combining intrinsic frequency $\omega_0 = (k/m)^{1/2}$ and quality factor $Q = (k/m)^{1/2}/c$, it is easy to yield the transfer function of an accelerometer with Laplace's transformation:

$$H(s)=\frac{x(s)}{a(s)}=\frac{1}{s^2+\frac{c}{m}s+\frac{k}{m}}=\frac{1}{s^2+\frac{\omega_0}{Q}s+\omega_0^2} \quad (17)$$

When working frequency is much lower than ω_0, the relationship between displacement and acceleration is simple:

$$x\propto\frac{1}{\omega_0^2}a=\frac{m}{k}a \quad (18)$$

This naturally leads to a trade-off between sensitivity and bandwidth, since the large resonance frequency required for high-speed operation results in vanishingly small displacements. In our design, the performance of high sensitivity is a central figure of merit, so we may take consideration of the displacement of the mechanical structure first instead of its resonance frequency.

3.1 The former design

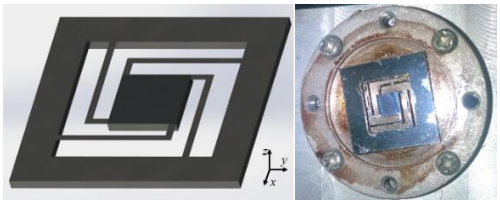

(a) (b)

Fig. 3: 3-D model and a photography of the former design

Figure 3 shows the former design of the mechanical structure, which consists of a bulk proof mass and four cantilevers. The top surface is covered with aluminum to serve as a reflecting mirror. Table 1 lists the parameters of the former mechanical structure [17].

Table 1. Parameters of the former mechanical structure

Size of cantilevers (two bends)	1000μm×300μm×10μm
length×width× thickness	5000μm×300μm×10μm
Volume of proof mass	3mm×3mm×415μm
Position of the cantilevers	Upper surface
Whole volume of structure	10mm×10mm×415μm

To compare with the performance of the former mechanical structure, I use a general purpose finite-element package ANSYS to analyze the maximum displacement and resonance frequency of both two designs.

When an acceleration of 1g (along z axis, which is the sensitive axis to acceleration) is applied to the former mechanical structure, the strain distribution and the maximum displacement can be solved by ANSYS. As is shown in figure 4. (a), the maximum displace under 1g acceleration along z axis is 53.1μm and the maximal von Mises stress is 45MPa. Combining the bending strength of single crystal silicon is 70MPa to 200MPa, the former design can stand the stress bought by $\pm$2~3g acceleration.

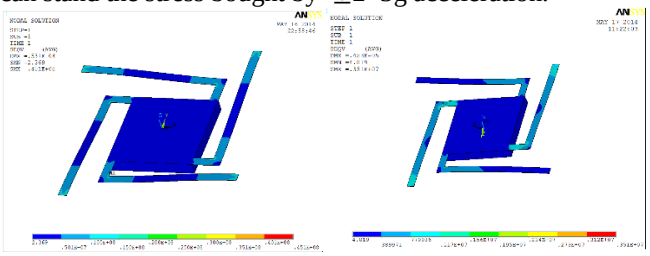

Fig. 4. (a): The deformation and stress distribution of former design with 1g acceleration along z axis (b) along x (y) axis

Table 2 shows the first five modes of former mechanical structure. It indicates that this structure has an inferior dynamic performance but fine static sensitivity of acceleration. An important performance in addition to the sensitivity is the crosstalk from other axis except sensitive axis to acceleration (here is x and y axis). The crosstalk from other axis can be described as:

$$Crosstalk=\frac{Displacement/1g\ on\ x(or\ y)\ axis}{Displacement/1g\ on\ z\ axis} \quad (19)$$

Table 2. First five modes of former mechanical structure

Number of modes	Resonance frequency/Hz
1	68.529
2	178.21
3	178.21
4	3362.3
5	3367.9

According to figure 4. (b), which is the deformation and stress distribution of the former mechanical structure with 1g acceleration acting on x axis, it is easy to get the crosstalk from x axis, the same to y axis:

$$Crosstalk=\frac{4.53\mu m}{53.1\mu m}=8.53\% \quad (20)$$

The crosstalk of former design cannot be tolerated actually. As a result of it, the modified mechanical design should take the sensitivity (maximum displacement) of the structure, the crosstalk from other axis and the resonance frequency into consideration.

3.2 The modified design

The modified mechanical structure is also based on a silicon-on-insulator (SOI) due to its mature process. To improve the performance of sensitivity and to reduce the crosstalk under the condition that material and the total size of this sensing structure is not changed, the parameters of cantilevers including length, width, thickness and the position of cantilevers should be redesign.

During the optimizing of the mechanic design, the first parameter that should be considered is the length of cantilevers (BL). According to the theory analyses, the displacement of sensing structure is proportional to the inverse square of the length of cantilevers. However, a simple increase of length will lead to the increase of the size of whole mechanical structure. Using multiple bends of cantilevers is a fairly common practice to increase the length of cantilevers in a same area.

The former design uses one bend, in view of the maximum von Mises stress should be less than 70MPa, choose three bends is reasonable. The simulation result is shown in figure 5, which indicates the displacement increase from 53.1μm to 107μm but the maximal von Mises stress is nearly invariable under 1g acceleration along *z* axis.

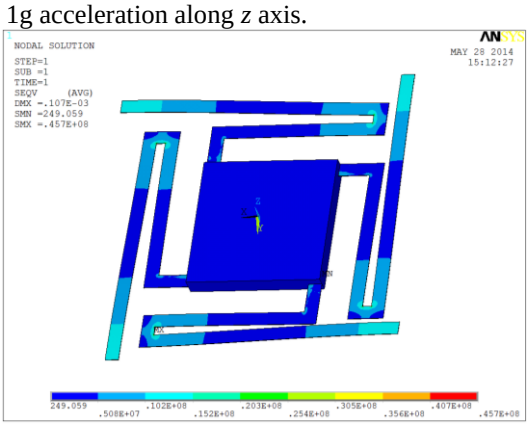

Fig. 5: The deformation and stress distribution of three bends design with 1g acceleration along *z* axis

Table 3 shows the first five modes of this mechanical structure with three bends. As displacement gains twice more, the dynamitic performance does not drop much.

Table 3. First five modes of mechanical structure with three bends

Number of modes	Resonance frequency/Hz
1	48.298
2	133.90
3	133.91
4	654.36
5	658.63

Then setting all parameters as table 1, but change the width of the cantilevers (BW) only when an acceleration of 1g is applied on the proof mass, the relationship between the width and displacement as well as the maximal von Mises stress is shown in figure 6. It indicates the fitting formula about BW and displacement is:

$$Dis = 2^{-8} BW^{-1.098} \mu m \tag{21}$$

The correlation coefficient of this power exponent formula is R^2=0.9997, which means this simulation fits the theory well. The theory analyses indicate that the displacement is inversely proportional to the width of a beam in this second-order harmonic oscillator system [18].

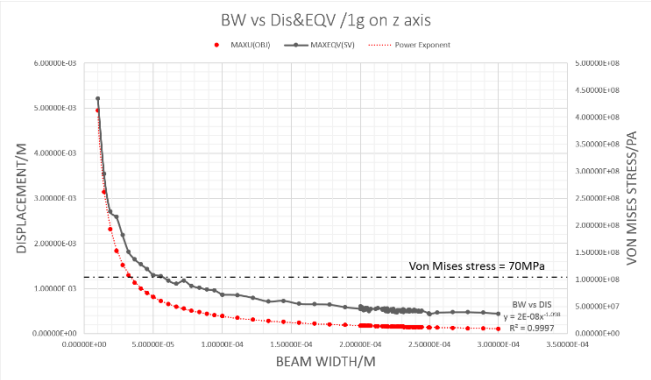

Fig. 6: Simulation of the displacement and maximum von Mises stress as functions of BW under 1g acceleration

The realization of improving the sensitivity of sensing structure, the width of cantilevers should be decreased indeed. However, the maximum von Mises stress determines the lower limit of the minimum width of cantilevers, as shown in figure 6, is about 50μm. Take account of other parameters which should be modified, the width of cantilevers is much bigger than 50μm in practice.

The relationship between resonance frequency and BW conveys that the resonance frequency changes little when the width of cantilevers decrease, as is shown in figure 7. Nonetheless, the width of cantilevers cannot be very small as the low-g accelerometer still needs tens of Hz to keep its dynamic performance.

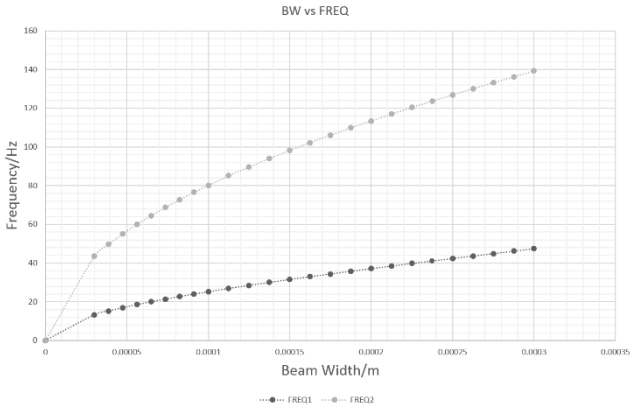

Fig. 7: The resonance frequency of first two modes as a function of BW under 1g acceleration

When it comes to the thickness of cantilevers (BT), I remain the other parameters except BT and only change BT. The relationship between the thickness and displacement as well as the maximal von Mises stress is shown in figure 8. The power exponent fitting formula is:

$$Dis = 2^{-19} BT^{-2.984} \mu m \tag{22}$$

Whose correlation coefficient is R^2=1. This fitting formula is according to the theory analyses perfectly, which indicates the displacement is inversely proportional to the three party of the thickness of cantilevers. Similar to the width of cantilevers, the maximum von Mises stress determines the upper limit of the minimum thickness of cantilevers. Because the trend of displacement and von Mises stress is quite alike, the lower limit of the thickness is about 8μm.

The relationship between resonance frequency and BT conveys that the second mode's downtrend is much bigger than that of the first mode when the width of cantilevers

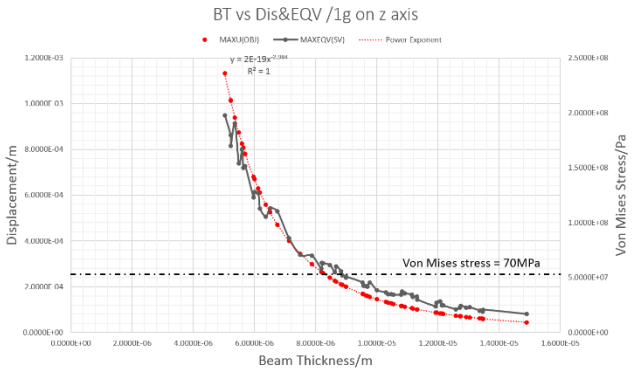

Fig. 8: Simulation of the displacement and maximum von Mises stress as functions of BT under 1g acceleration

decrease, as is shown in figure 9. To keep enough dynamic property that is concerned to the frequency gap between first mode and second mode, the thickness of cantilevers cannot be very small.

Combining the thickness of Handle Silicon in SOI, it is acceptable to change the thickness of cantilever little.

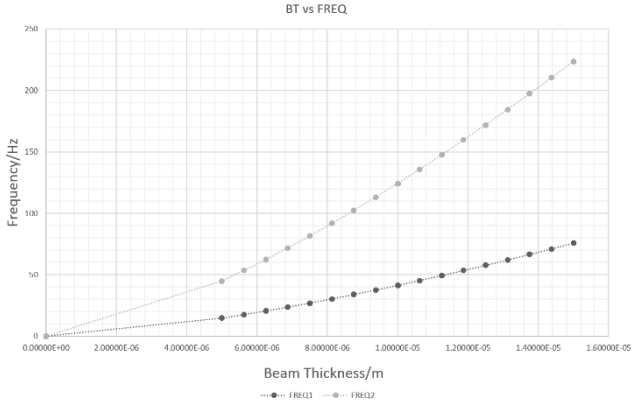

Fig. 9: The resonance frequency of first two modes as a function of BT under 1g acceleration

To reduce the crosstalk of sensing structure, a modification of the position of cantilevers is required. The theory analysis indicates that the more symmetrical a structure is, the less crosstalk there will be. The simulation results accords quite well with the theory analysis. When the position of cantilevers moves from the upper surface to the centre of the proof mass, the crosstalk falls to 0.036% from 7.84% dramatically, as is shown in figure 10. Changing the position of cantilevers can perfectly suppress crosstalk without degradation of other performance, though it may add complexity of SOI and process.

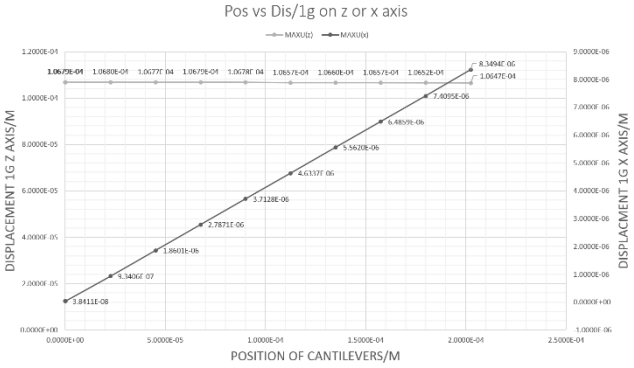

Fig. 10: The displacement concerned to the position of cantilevers under 1g acceleration along z or x axis

Synthesize the length, width, thickness and position of cantilevers, I finally optimize the parameters of mechanical design to table 4 according to the displacement, maximum von Mises stress and crosstalk. Figure 11 (a), (b) show the deformation and stress distribution of modified design with 1g acceleration along *z* axis and *x* axis respectively. Table 5 lists the properties of modified mechanical design compared to the former design. This modified design increases the displacement under 1g acceleration along z axis by almost three times and decreases the crosstalk to less than a hundredth of the former one. This modified design can stand proportional acceleration as the former design with similar dynamic performance as shown in table 5.

Table 4. Parameters of the modified mechanical structure

Size of cantilevers (three bends) length×width× thickness	1400μm×240μm×10μm 3900μm×240μm×10μm 800μm×240μm×10μm 5900μm×240μm×10μm
Volume of proof mass	3mm×3mm×415μm
Position of the cantilevers	Centre of proof mass
Whole volume of structure	10mm×10mm×415μm

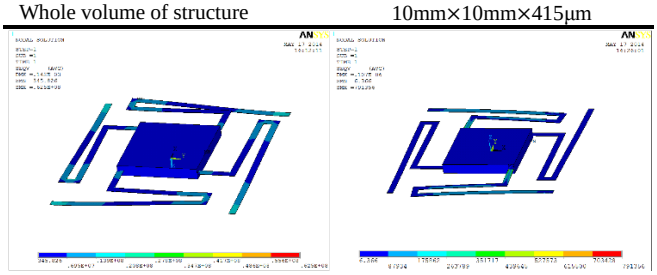

Fig. 11. (a): The deformation and stress distribution of modified design with 1g acceleration along *z* axis (b) *x* axis

To protect this mechanical structure from a huge acceleration, two baffles are imported to our design. In consideration of the maximum acceleration this structure can support, I set the distance between baffles and proof mass to 200μm and the thickness of baffles to 100μm.

Table 5. The properties of modified mechanical design compared to the former design

	Displacement	**Stress**	**Crosstalk**	**1st Resonance Frequency**
The former design	53.1μm	45MPa	8.53%	68.529Hz
The modified design	143μm	63MPa	0.075%	41.812Hz

The schematic of final design is shown in figure 12, which can be made by a single SOI chip. Here I add a plane-parallel plate capacitor composed of two metal films on underside of the proof mass and upper surface of baffle, which serves as a realization of feedback.

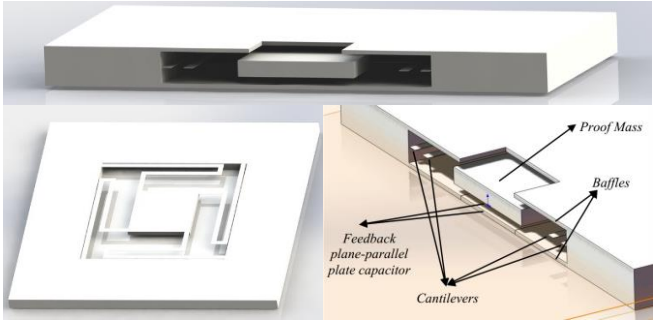

Fig. 12: The cross-section drawn of the modified design

Combining table 5 and former experimental results [17], as is shown in figure 13, we have reason to believe the peak slope of output will be much larger than 1676 V/g and the resolution of this design will be higher than 1μg (as the peak-to-peak noise level is 2mV). In addition, the modification of cantilevers' position will effectively suppress the variation of peak-to-peak value of output voltage because the crosstalk is perfectly decreased, as is shown in figure 14.

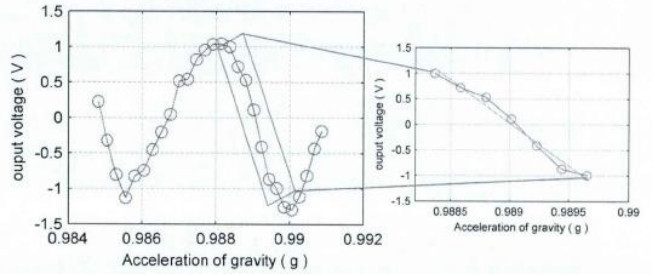

Fig. 13: The former static gravitational acceleration measurement result

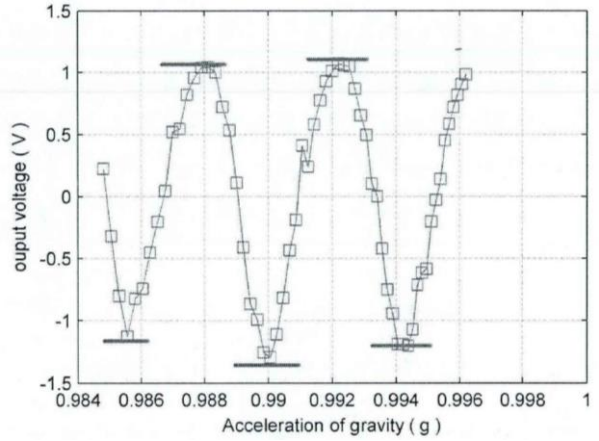

Fig. 14: The variation of peak-to-peak value of output voltage brought by crosstalk

4. CONCLUSIONS

We have demonstrated an improved MOEMS accelerometer based on integrated grating with phase modulation scheme. The parameters of mechanical structure are redesigned to increase the sensitivity and to decrease the crosstalk of this sensing chip. Compared to the former design we have fabricated, this modified design is likely to have a higher sensitivity of 3×10^3V/g corresponding to a resolution higher than 1μg. For an accelerometer, the stability of temperature is required to make it keep a steady performance. In a whole acceleration detection system, we have applied an intelligent PID temperature control which is composed of several TECs and a PID circuit. In the future, an electrostatic force feedback will be employed to achieve a closed-loop system, which can keep the sensitivity at the maximum point and increase the dynamic range and bandwidth. Finally, the processing circuit, VCSEL and sensing chip can be integrated in one microchip.

ACKNOWLEDGEMENTS

The author would like to thank Professor Bai Jian and Yang Guoguang for help in the research, thank Lian Wenxiu and Lou Shuqi for the support in the experiment and acknowledge all the staff of the State Key Laboratory of Modern Optical Instrumentation, Zhejiang University.

REFERENCES

[1] A. R. Schuler and K. A. Fegley, "Measuring rotational motion with linear accelerometers," IEEE Trans. Aerosp. Electron. Syst. AES-3, 465–472 (1967).

[2] B. E. Boser and R. T. Howe, "Surfaced micromachined accelerometers," IEEE J. Solid-State Circuits 31, 366–375 (1996).

[3] N. Yazdi, F. Ayazi, and K. Najafi, "Micromachined inertial sensors," Proc. IEEE 86, 1640–1659 (1998).

[4] G. A. Macdonald, "A review of low cost accelerometers for vehicle dynamics," Sens. Actuators A 21, 303–307 (1990).

[5] Y. Wu and X. Zeng et al., "MOEMS accelerometer based on microfiber knot resonator", Proc. of SPIE 7503(75036), (2009).

[6] C. Hou and Y. Wu et al., "Novel high sensitivity accelerometer based on a microfiber loop resonator", Opt. Eng. 49(1), 014402(2010).

[7] Y. Wu and X. Liu et al., "Structure Design of MI-Z Interference MOEMS Accelerometer", International Technology and Innovation Conference, 1801-1807(2006).

[8] M. Stephens, "a sensitive interferometric accelerometer", Rev.Sci.Instrum. 64(9), 2612-2614(1993).

[9] K. Zandi and B.Wong et al., "In-plane silicon-on-sulator optical MEMS accelerometer using waveguide Fabry-Perot microcavity with silicon/air bragg mirrors", IEEE Conference on MEMS,839-842(2010)

[10] L. Feng and H. Liu et al., "MOEMS accelerometer based on double Fabry-Perot interferometers and closed loop", Journal of Beijing University of Aeronautics and Astronautics 32(6), 691-694(2006).

[11] Neal A. Hall, Murat Okandan, Robert Littrell, Darwin K. Serkland, Gordon A. Keeler, Ken Peterson, Baris Bicen, Caesar T. Garcia, and F. Levent Degertekin, "Micromachined Accelerometers With Optical Interferometric Read-Out and Integrated Electrostatic Actuation", JOURNAL OF MICROELECTROMECHANICAL SYSTEMS, vol.17(1), pp. 37-43, 2008

[12] Liuhua Chen, Qiao Lin, Shu Li, and X. Wu, "Optical accelerometer based on high-order diffraction beam interference", APPLIED OPTICS, vol. 49(14), pp. 2658-2664, 2010

[13] E. B. Cooper and E. R. Post et al, "high-resolution micromachined interferometric accelerometer", Applied Physics Letters 76(22), 3316-3318(2000).

[14] N. A. Hall and M. Okandan et al, "micromachined accelerometers with optical interferometric read out and integrated electroelastic actuation", Journal of Microelectromechanical systems 17(1), 37-44(2008).

[15] N. C. Loh and M. A. Schmidt et al., "sub-10 cm3 interferometric accelerometers with nano-g resolution", Journal of Microelectromechanical systems 11(3), 182-187(2002).

[16] S. R. Manalis, S. C. Minne, A. Atalar, and C. F. Quate, "Interdigital cantilevers for atomic force microscopy", Appl. Phys. Lett. 69, 3944–3946 (1996).

[17] Shuangshuang Zhao and Juan Zhang et al., "Optical accelerometer based on grating interferometer with phase modulation technique", APPLIED OPTICS, vol. 51(29), pp. 7005-7010, 2012

[18] Mineta, T and Kobayashi, S et al, "Three-axis capacitive accelerometer with uniform axial sensitivities", JOURNAL OF MICROMECHANICS AND MICROENGINEERING, vol. 6(4), 431-435, 1996